Journal of ELECTRICAL ENGINEERING, VOL 73(2022), NO3, 166–173

sciendo

PAPERS

Compact triple-band implantable antenna for multitasking medical devices

Ömer Faruk Çelik[1], **Sıddık Cumhur Başaran**[2,1]

This paper presents a compact implantable antenna's design, fabrication, and measurement for biotelemetry applications. The proposed design with the size of 255 mm^3 provides a triple-band operation that covers all the Medical Implant Communication Service (MICS: 402 MHz), Medical Device Radiocommunications Service (MedRadio: 405 MHz), and Industrial, Scientific, and Medical (ISM: 433, 915 and 2450 MHz) bands simultaneously. The compact structure with triple-band performance is essentially achieved by using a spiral-like radiator loaded with meandered and internal gear-shaped elements excited by a vertical coaxial probe feed. Also, the slots-loaded partial ground plane is utilized to improve impedance matching at the desired frequency bands. The design and analysis of the antenna were carried out using the Ansoft HFSS software in a homogenous skin model and the CST Microwave Studio in a realistic human model. The proposed antenna was fabricated to validate the simulated results, and characteristics of its return loss and radiation patterns were measured in minced pork meat. Moreover, realized gains and specific absorption rate (SAR) values of the antenna were numerically computed using the simulators. Based on the simulated and measured results, the proposed antenna performance was found to be comparable to the limited number of multiband implantable antenna designs reported in the recent literature.

K e y w o r d s: biotelemetry applications, implantable antennas, ISM bands, MedRadio bands, triple-band antennas

1 Introduction

In-body medical devices (IBMDs) that dynamically transmit the physiological parameters they receive from inside the human body to an external unit are used in various applications such as neural recording [1], cardiac pacemaker [2], monitoring glucose [3] and intraocular pressure [4], and capsule endoscopy [5]. For these applications to be realized simultaneously, multiband implantable antennas operating in the frequency bands allocated for biotelemetry applications are needed. In addition, implantable antennas should be as compact as possible to adapt to miniaturized IBMDs. Moreover, due to the high loss of the in-body environment, the gain of implant antennas is expected to be as high as possible. On the other hand, these antennas must meet the specific absorption rate (SAR) limitations determined by international standards.

Medical telemetry applications are primarily carried on in the MICS (402 – 405 MHz) and MedRadio (401 – 406 MHz) bands. In addition to these bands, Medical Telemetry Service (WMTS: 1395 1400 MHz, and 1427 1432 MHz) bands are also allocated for the applications. Apart from these bands, the ISM bands (433 -436 MHz, 902 -928 MHz, and 2.4 -2.484 GHz) are frequently preferred for this application due to not requiring any license.

Single-band, dual-band, or multiband implantable antenna designs of various types and specifications that can meet the principal requirements of IBMDs have been reported in the literature [6-25]. In this context, single-band, and dual-band implantable antenna based on split-ring resonator (SRR), which are the building blocks of metamaterial structures, have been designed in [6] and [7], respectively. In addition, complementary SRRs have been used as the primary radiator to achieve a dual-band implantable antenna in [8]. Stack antenna configurations based on - shaped [9] and S-shaped [10] radiator have been developed for multiband implantable operations. For the same purpose, two different implantable antennas with serpentine-shaped resonators have been designed in [11] and [12]. To achieve a miniature implantable antenna structure offering dual-band operation, meandered resonators have been employed in [13] and [14]. Similarly, multiband miniaturized implantable antennas with spiral-shaped resonators have been designed in [15] and [16]. On the other hand, circularly polarized implantable antennas have been reported in [17] and [18] for single-band in-body applications. In [19], implantable antennas based on effective relative permittivity calculation have been discussed.

In this paper, we propose a novel triple-band compact implantable antenna for multi-tasking in-body medical devices. The radiator of the suggested antenna consists of three semi circular-shaped concentric resonators that are spirally connected and a circular patch placed in their center. This configuration utilizes to keep a sizeable current path in a limited area, and thus miniatur-

[1] Karadeniz Technical University, Department of Electronics and Communications Engineering, Trabzon, 61830, Turkey, [2] Akdeniz University, Department of Electrical-Electronics Engineering, 07058 Antalya, Turkey, [1] cbasaran@akdeniz.edu.tr

https://doi.org/10.2478/jee-2022-0022, Print (till 2015) ISSN 1335-3632, On-line ISSN 1339-309X

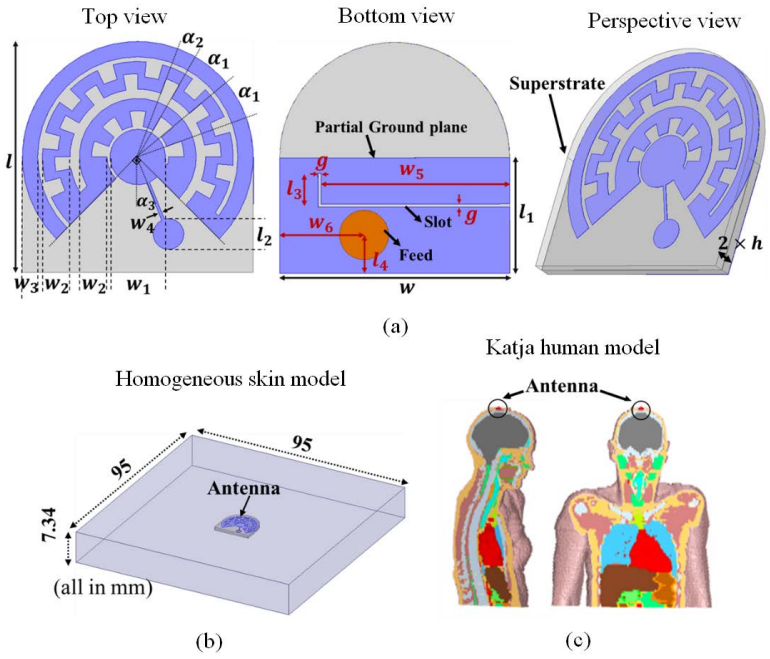

Fig. 1. Proposed antenna structure and simulation environment: (a) – top, bottom, and perspective views of the antenna,(b)(a) – homogenous skin model, and (c) – a realistic human model

ization is achieved. Thanks to the meandered structures used on the resonators that excite main frequency modes, the current paths are extended, and additional miniaturization is provided. Also, a partial ground plane loaded with an L-shaped slot is used to improve impedance matching and adjust resonant frequencies. As a result, the proposed antenna with the novel structure operates at 433MHz (392-474MHz), 921.5 MHz (843-1000MHz), and 2405 MHz (2.02-2.76GHz). Thus, it completely covers MICS (402 MHz), MedRadio (405 MHz), and ISM (433, 915, and 2450 MHz) bands, where all bands can be used for biotelemetry applications. Also, the antenna exhibits comparable size, bandwidth, realized gain, and SAR distribution performance with the recently reported multiband implantable antennas. In this article, the proposed antenna structure is introduced in detail, the design evolution stages based on its equivalent circuit model are explained, and the simulated and measured antenna performance is presented, respectively.

2 Trible-band implantable antenna and performance analysis

In this section, firstly, the structure of the proposed antenna and simulation environments are introduced in detail. Then, design evolution stages are discussed based on the lumped element equivalent circuit model, and the current distributions at the related frequencies are given. Finally, the simulated and measured characteristics of the proposed antenna are presented, and the antenna's performance is compared with other reported multiband antennas.

2.1 Proposed antenna structure and simulation environments

The proposed antenna structure and the simulation environments are illustrated in Fig. 1, while its design parameters and corresponding values are given in Tab. 1. As shown in Fig. 1(a), the primary radiator of the antenna is composed of three concentric semi-circular ring resonators of different structures connected spiral-like, and a fully circular-shaped patch placed in their center. The outermost resonator has a straight profile, while the innermost is an internally gear-shaped structure. The resonator between them is in the form of a meandered line. The antenna is excited by a thin microstrip feed line placed between the circular patch and feeding point. The radiator with microstrip feed line is on a single-layer semi-circular Rogers RO3010 substrate ($\varepsilon_r = 10.2$ and $\tan\delta = 0.0022$) with 0.635 mm thickness. The radiator is excited by a vertical coaxial probe feed placed between the feed line and the ground plane. A partial ground plane loaded with an L-shaped slot is placed on the backside of the substrate, as shown in Fig. 1(b). In addition, the Rogers RO3010 copper-free pure dielectric material is utilized as a top layer (superstrate) to prevent the direct connection between the body tissue and copper radiator.

This suggested compact design achieves the triple-band operation using the spiral-shaped radiator with various semi-ring resonators. At the same time, bandwidth improvement and fine frequency adjustment are provided thanks to the slot-loaded partial ground plane. Numerical design and analysis were conducted using the HFSS simulation setup that mimics a homogenous skin model, as shown in Fig.1(b). The electrical properties of the ho-

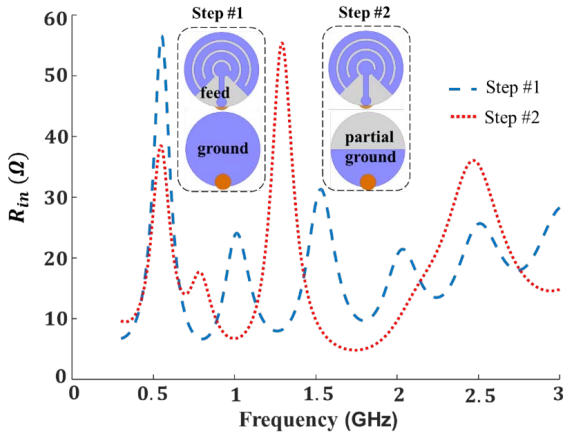

Fig. 2. Design steps(#1 and #2)of the proposed antenna and corresponding real parts of the input impedance characteristics

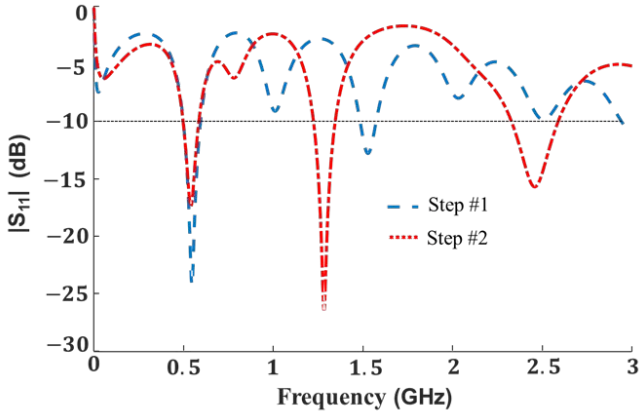

Fig. 3. Return loss characteristics for the proposed antenna design steps #1 and #2

mogeneous skin tissue were assigned in the simulator depending on the frequency. The skin tissue's dielectric constant and conductivity values were $\varepsilon_r = 46.74$ and $\sigma = 0.689\,\mathrm{S/m}$ at 402 MHz, $\varepsilon_r = 41.33$ and $\sigma = 0.872\,\mathrm{S/m}$ at 915 MHz, $\varepsilon_r = 38.01$ and $\sigma = 1.46\,\mathrm{S/m}$ at 2450 MHz, respectively, [20]. In addition, the optimum antenna structure was again analyzed using the CST Katja realistic human model, shown in Fig. 1(c), for additional validation. In both simulators, the antenna was positioned at a depth of 3 mm.

Table 1. Design parameters of the proposed antenna

Parameter	Value (mm)	Parameter	Value (mm)
w	15	l_1	7.5
w_1	3.6	l_2	2
w_2	1.8	l_3	2.2
w_3	1	l_4	2.5
w_4	0.2	α_1	20°
w_5	12.3	α_2	10°
w_6	5.5	α_3	22°
l	15	g	0.2

2.2 Design evolution based on the resonance principle and equivalent circuit model

This compact antenna configuration providing triple-band performance was developed in four main steps. Also, many parametric studies were carried out to adjust the desired resonance frequencies simultaneously, and optimum design parameters were obtained. The configurations of the first two design steps (#1 and #2) and the impedance characteristics corresponding to each step are shown in Fig. 2. Also, the return loss characteristics of the configurations are illustrated in Fig. 3. As seen in Fig. 2, the starting configuration of the antenna consists of a three windings spiral-shaped radiator placed on a dielectric substrate with the other side fully grounded. The antenna is excited by the microstrip feed line connected to the circular patch in the center of the radiator. Each winding of the spiral-shaped radiator and the circular patch

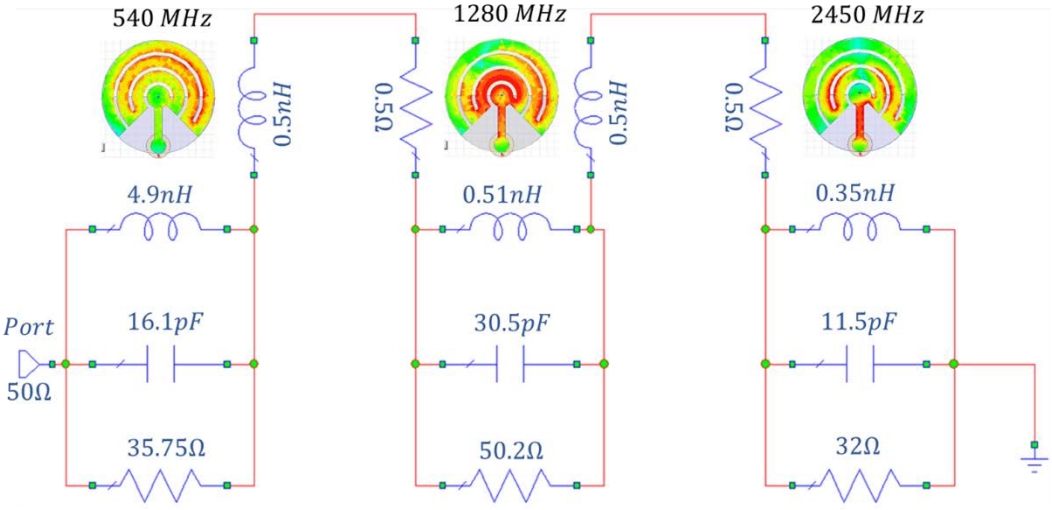

Fig. 4. Equivalent circuit model for step #2

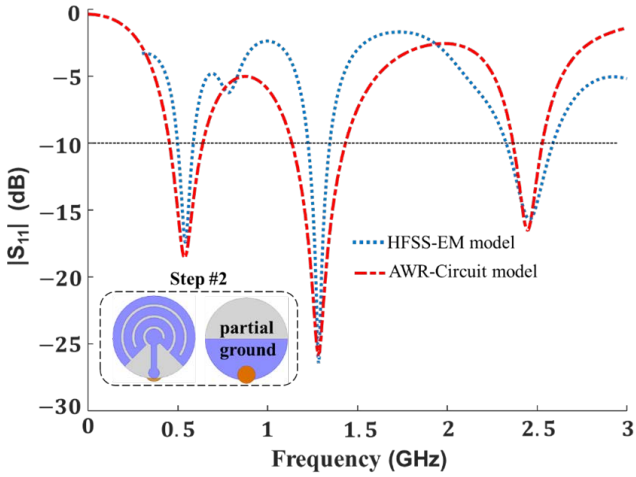

Fig. 5. Simulated return loss characteristics of EM and circuit model for step #2

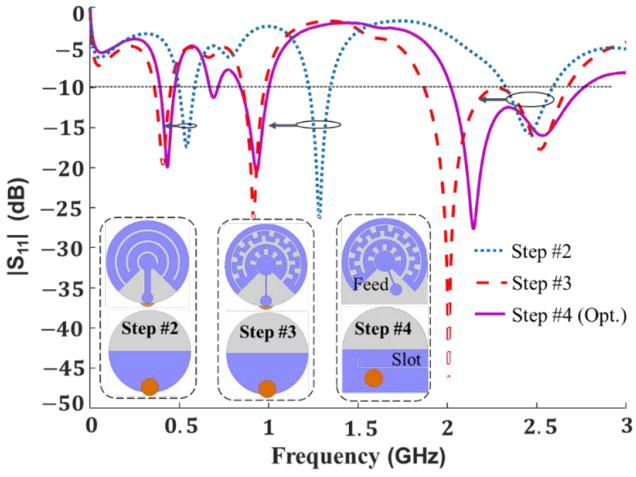

Fig. 6. Return loss(s11)characteristics for configurations #2 and #3 of the antenna

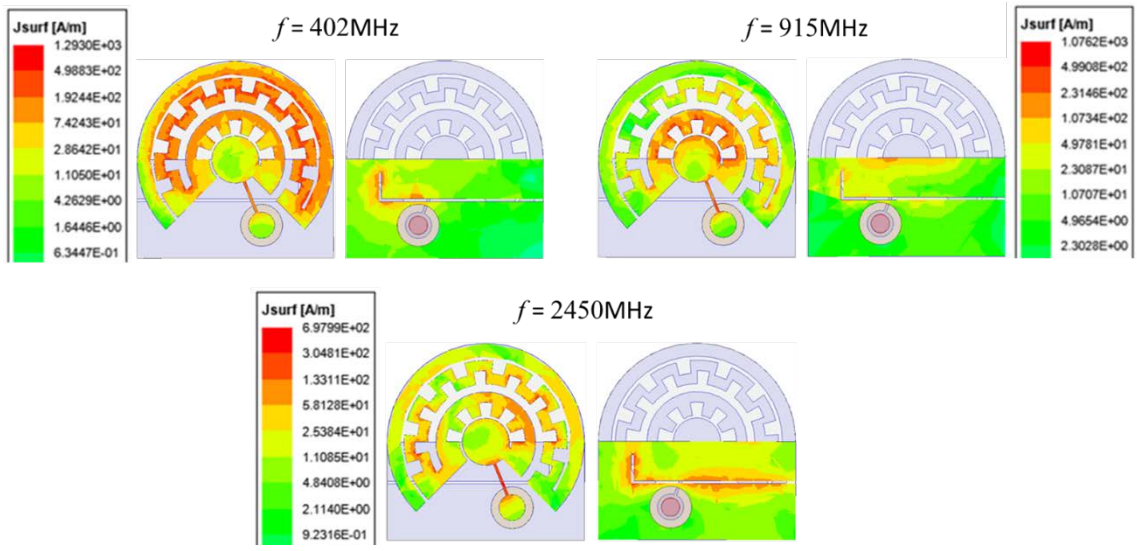

Fig. 7. Surface current distributions for the proposed antenna

act as a resonator, exciting a different resonant mode. Figure 2 and 3 show that the starting configuration exhibits multi-band behavior. However, since the impedance values are low (about 20-30 ohms) at frequencies other than 500 MHz, full resonant modes do not occur at these frequencies. Therefore, a partial ground plane is introduced to the antenna (step #2) to tune the impedance levels (about 40-50 ohm), as shown in Fig. 2. Hence, the configuration (#2) offers a triple-band operation with sufficient bandwidths at 540, 1280, and 2450 MHz, respectively, as shown in Fig. 3.

Figure 4 shows surface current densities of configuration #2 at the resonance frequencies and its lumped equivalent circuit model obtained using AWR-Microwave Office Circuit Design Software. The AWR simulated return loss characteristic is compared with the HFSS result, as illustrated in Fig. 5. An excellent agreement is achieved. When surface current densities at the resonant frequencies shown in Fig. 4 are examined, as expected, the current is concentrated in the outermost resonators. Thus, the first frequency band (540 MHz) occurs because of the effective lengths of the resonators. The innermost resonators excite the second frequency band at about 1280 MHz. Also, the third frequency band (2450 MHz) is mainly generated by the microstrip feed line. Based on the current distributions and resonance principle, lumped elements equivalent circuit of configuration #2 is modeled as three resonators connected in series. It can be seen that each resonator is modeled as an RLC circuit, and the series connection between them is modeled as an RL circuit. The optimal values of RLC are provided using the AWR software.

We now discuss the other design stages (#3 and #4) that resulted in the desired antenna structure operating at 402, 915, and 2450 MHz frequencies used for biotelemetry applications. Figure 6 shows the configuration of steps

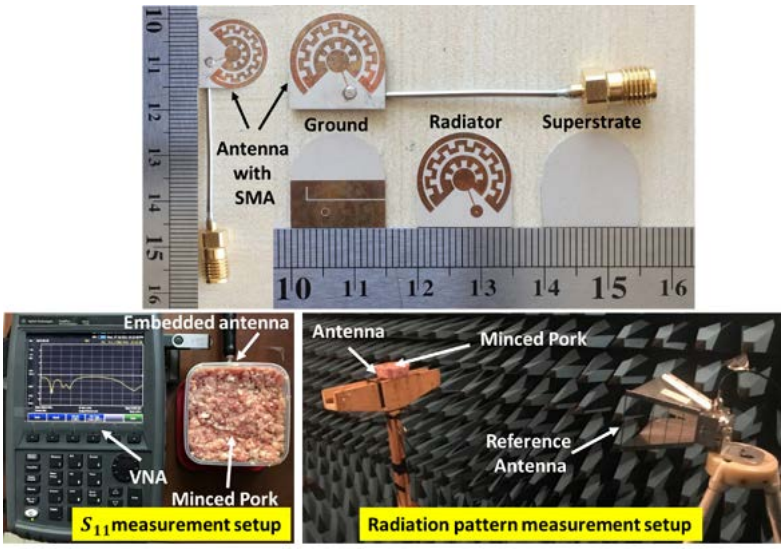

Fig. 8. Photographs of the antenna prototypes and measurement setups

(#2, #3, #4) and compares their frequency responses. As seen, the current path is extended, and the frequency bands are shifted to the lower value by using the meandered line and internally geared shaped structure in the second and third rings, respectively, in Step#3. Thus, 402 MHz, 915 MHz, and 2 GHz bands are achieved thanks to this configuration. However, impedance matching at 2.45 GHz needs to be improved to obtain a better resonance characteristic. Finally, the circular ground plane is enlarged by replacing it with a square type to increase realized

The gain of the design (see Step #4). And thus, approximately 2.5 dBi, the gain improvement is achieved at 402 and 915 MHz frequencies. Also, an L-shaped slot is introduced on the ground plane, and the feed point is shifted to the right side to precisely adjust the desired frequency bands. The optimum size and location of the slot and position of the feed point have been determined by a series of parametric studies and the surface current distributions.

2.3 Surface current distributions

To evaluate the resonance principle, the simulated surface current distributions at each resonant mode are presented in Fig. 7. It can be seen that the current distribution is concentrated on the two outermost ring resonators at 402 MHz, as expected. For 915 MHz, it has a high concentration on the gear-shaped resonator. Next, the current distribution at 2450 MHz is concentrated on the right side of the gear-shaped resonator, microstrip feed line, and the slot placed on the ground plane.

3 Results and discussion

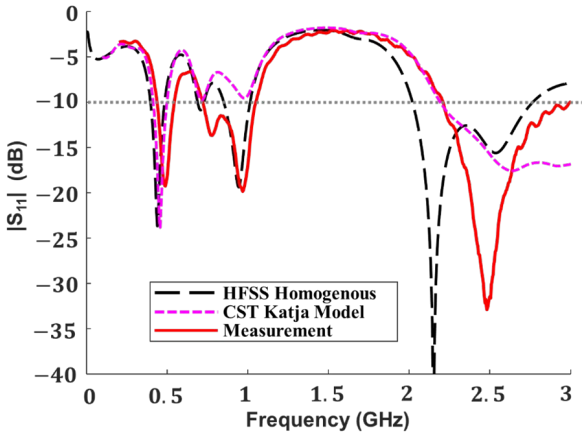

Fig. 9. Comparisons of the simulated and the measured return loss characteristics for the antenna

The proposed implantable antenna design was fabricated, and the prototype antenna's return loss and radiation pattern measurements were carried out. Fig. 8 shows the prototype antennas and the measurement setups of return loss and radiation patterns. As seen, the measurements were performed by immersing the prototype in the minced pork meat. The prototype antenna was placed at a depth of about 3mm in the meat. The simulated and measured return loss characteristics are illustrated in Fig. 9. The simulation of the antenna in a homogenous skin model was carried out using the Ansoft HFSS simulator. The simulation was repeated using the CST Katja realistic human model for additional validation, as shown in Fig. 1(c). It can be seen that the simulation and measurement results are in good agreement, except for a slight level shift of the Katja model at 915 MHz. Based on the HFSS result, the proposed antenna operates at 433 MHz, 921.5 MHz, and 2405 MHz frequencies with corresponding impedance bandwidths of 18.94%, 17.04%, and 30.96%, respectively. As a result, the antenna simultaneously covers licensed (MICS 402 MHz

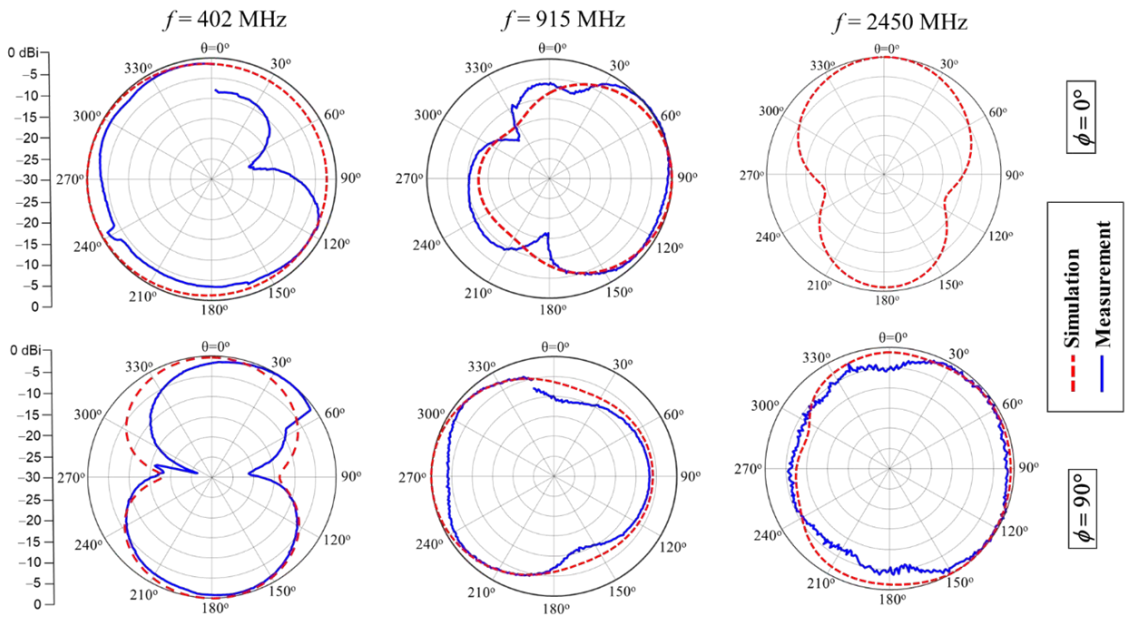

Fig. 10. Comparisons of the simulated and the measured radiation patterns for the antenna

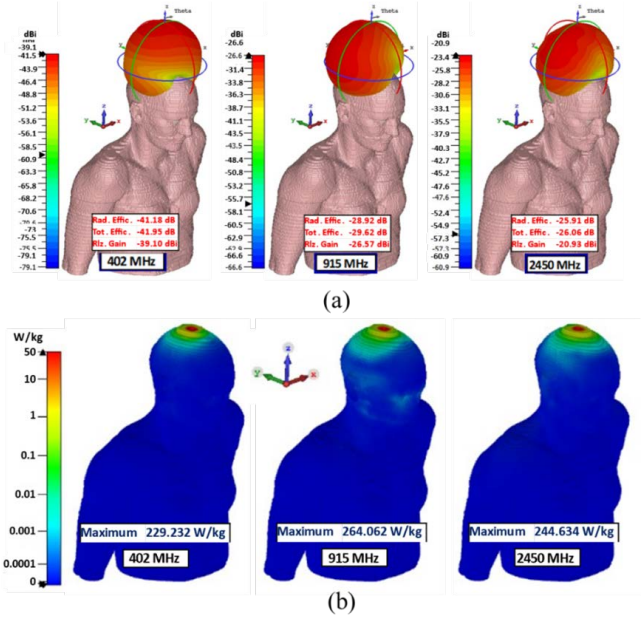

Fig. 11. Antenna simulations inside Katja realistic human model: (a) – radiation patterns,(b) – SAR distributions(the values are normalized plotted)

and MedRadio 405 MHz) and free (ISM 433, 868, 915, and 2450 MHz) frequency bands for biotelemetry applications. Thanks to the use of ISM bands in addition to MedRadio bands, multiple biotelemetry applications can be performed simultaneously.

Radiation patterns of the antenna simulated in the homogenous model and measured in the minced meat from pork are displayed in Fig. 10. It is observed that the simulation and measurement results are in good agreement, except for minor differences in some cases, probably due to the deterioration of minced meat during the long measurement period. In addition, while measuring the radiation pattern of the antenna for $\phi = 0$ at 2450 MHz, the measurement could not be completed due to the failure of the positioner controller device.

Also, realized gain values of -33.76, -16.8, and -21.2 dBi are obtained at 402, 915, and 2450 MHz. On the other hand, Fig. 11 shows the radiation patterns and SAR distributions obtained using CST Katja realistic human model for additional validation. As shown in Fig 11 (a), the peak realized gain values at 402, 915, and 2450 MHz are -39.1, -26.57 and -20.96 dBi, respectively. Also, the obtained SAR values for 0.5 W input power are about 229, 264, and 245 W/kg for these frequencies, as shown in Fig 11 (b). The simulated peak SAR values seem to be high as compared to the standard imposed by the IEEE. How-

Table 2. Performance comparison of the multiband implantable antennas

Ref.	Frequency bands (MHz)	Bandwidth (%)	Peak Gain (dBi)	Volume (mm^3)	1-g Avg SAR (W/kg)
(10)	MICS&MR&ISM(433)	37.3	-22	254	N/A
	WMTS (1430)	3.64	-17		
	ISM (2450)	4.16	-16		
(11)	MICS&MR	15.92	-40.85	52.5	665
	ISM (915)	9.95	-32.98		837
	ISM (2450)	4.29	-22.37		759
(12)	ISM (915)	8.7	-26.4	21	380
	Midfield (1800)	8.2	-23		358
	ISM (2450)	7.3	-20.47		363
(15)	MICS&MR&ISM(433)	36.8	-30.5	17.15	305
	Midfield (1600)	10.69	-22.6		588
	ISM (2450)	8.94	-18.2		305
(16)	MICS&MR	23.13	-23	197.04	241
	WMTS (1430)	14.13	-20.5		269
	ISM (2450)	18.12	-19		290
(21)	MICS&MR&ISM(433)	24.81	-12.25	432	1299
	ISM (2450)	14.7	-12.4		990
(22)	MICS&MR&ISM(433)	30	-18.5	447	N/A
	ISM (2450)	1.6	-19.5		
(23)	MICS&MR&ISM(433)	28	-16	340	242
	ISM (2450)	10	-13.8		150
This work	MICS&MR&ISM(433)	18.94	-33.76	255	229
	ISM (915)	17.04	-16.8		264
	ISM (2450)	30.96	-21.2		245

MR: MedRadio

ever, the maximum input power for implantable medical devices is restricted to 25 μW. In this context, we calculate the maximum allowable input power to meet the 1-g SAR safety limits. To keep the SAR values under the IEEE standards, the proposed antenna allows maximum input power of 3.49 mW at 402 MHz, 3.03 mW at 915 MHz, and 3.26 mW at 2450 MHz. Based on the restricted input power of 25 μW, the proposed antenna is safe for operation in all bands.

In this section, the proposed triple-band implantable antenna design is compared with the previously reported multiband implantable antennas in terms of the volumes, operating frequencies, impedance bandwidths, gains, and SAR distributions. In this context, Tab. 2 shows the detailed performance comparison of the antennas. As seen, only the proposed antenna simultaneously covers MICS (402 MHz), MedRadio (405 MHz), and ISM (433, 915, and 2450 MHz) bands allocated for biotelemetry applications. Also, the proposed antenna has the lowest SAR distribution values compared to the others. Moreover, the proposed antenna performs comparably to other antennas in terms of bandwidth, gain, and size. Furthermore, unlike the reported implantable antennas, only in this study the resonance modes of the antenna are explained based on the lumped element equivalent circuit model.

4 Conclusion

In this study, a triple-band implantable antenna loaded with various shaped concentric resonators, each exciting a different resonant mode, was designed for multi-purpose biotelemetry applications. Also, a lumped equivalent circuit model of the suggested antenna was developed to demonstrate the working mechanism and behavior of the excited modes. Moreover, the fabricated prototype's return loss and radiation pattern measurements were performed inside the minced meat from pork to validate the numerical results. According to the return loss characteristics, only the proposed antenna simultaneously covers MICS (402 MHz), MedRadio (405 MHz), and ISM (433, 915, and 2450 MHz) bands used for biotelemetry applications when compared to the other reported multiband implantable antennas. In addition, SAR distribution and realized gain values in the respective bands are better than the most of the said antennas.

References

[1] T. Karacolak, A. Hood, and E. Topsakal, "Design of a dual-band implantable antenna and development of skin mimicking gels

for continuous glucose monitoring", *IEEE Transaction on Microwave Theory and Technique*, vol. 56, no. 4, pp. 1001-1008, 2008.

[2] H. Bhamra, J.-W. Tsai, Y.-W. Huang, Q. Yuan, J. V. Shah, and P. A. Irazoqui, "Subcubic millimeter wireless implantable intraocular pressure monitor microsystem", *IEEE Transactions on Biomedical Circuits and Systems*, vol. 11, no. 6, pp. 1204-15, 2017.

[3] Z. Bao and Y.-X. Guo, "Novel miniaturized antenna with a highly-tunable complex input impedance for capsules", *IEEE Transactions on Antennas and Propagation*, vol 69, no. 6, pp. 3106-3114, 2020.

[4] S. M. Asif, A. Iftikhar, B. D. Braaten, D. L. Ewert, and K. Maile, "A wide-band tissue numerical model for deeply implantable antennas for RF-powered leadless pacemakers", *IEEE Access*, vol. 7, pp. 31031-42, 2019.

[5] H. Bahrami, S. A. Mirbozorgi, R. Ameli, L. A. Rusch, and B. Gosselin, "Flexible, polarization diverse UWB antennas for implantable neural recording systems", *IEEE Transactions on Biomedical Circuits and Systems*, vol. 10, no. 1, pp. 38-48, 2015.

[6] A. Sondas and M. H. B. Ucar, "An implantable microstrip antenna design for MICS-band biomedical applications", *Turkish Journal of Electrical Engineering Computer Sciences*, vol. 24, no. 4, pp. 2267-73, 2016.

[7] Y. E. Yamac and S. C. Basaran, "An SRR based miniature implantable antenna with a slit loaded ground at MedRadio and ISM bands for biotelemetry applications", *International Journal of RF and Microwave Aided-Computer Engineering*, vol. 30, no. 11, 2020.

[8] M. Usluer, B. Cetindere, and S. C. Basaran, "Compact implantable antenna design for MICS and ISM band biotelemetry applications", *Microwave and Optical Technology Letters*, vol. 62, pp. 1581-7, 2020.

[9] F. J. Huang, C. M. Lee, C. L. Chang, L. K. Chen, T. C. Yo, and C. H. Luo, "Rectenna application of miniaturized implantable antenna design for triple-band biotelemetry communication", *IEEE Transactions on Antennas and Propagation*, vol. 59, no. 7, pp. 2646-53, 2011.

[10] C. K. Wu, T. F. Chien, C. L. Yang, and C. H. Luo, "Design of novel S-shaped quad-band antenna for MedRadio/WMTS/ISM implantable biotelemetry applications", *International Journal of Antennas and Propagation*, vol, 2012.

[11] I. Gani and H. Yoo, "Multi-Band Antenna System for Skin Implant", *IEEE Microwave and Wireless Components Letters*, vol. 26, pp. 2946, 2016.

[12] M. Zada and H. Yoo, "A Miniaturized Triple-Band Implantable Antenna System for Bio- Telemetry Applications", IEEE Transactions on Antennas and Propagation, vol. 66, pp. 7378-82, 2018.

[13] M. Al-Hasan, P. R. Sura, A. Iqbal, J. J. Tiang, I. B. Mabrouk, and M. Nedil, "Low-profile dual band implantable antenna for compact implantable biomedical devices", *AEU-International Journal of Electronics and Communications*, vol. 138, pp. 1538-96, 2021.

[14] A. S. S. Ahson and Y. Hyoungsuk, "Scalp-implantable antenna systems for intracranial pressure monitoring", *IEEE Transactions on Antennas and Propagation*, vol. 66, no. 4, pp. 2170-73, 2018.

[15] I. A. Shah, M. Zada, and H. Yoo, "Design and analysis of a compact-sized multiband spiral-shaped implantable antenna for scalp implantable and leadless pacemaker systems", *IEEE Transaction on Antennas and Propagation*, vol. 67, no. 6, pp. 4230-34, 2019.

[16] T. A. L. Trong, S. I. H. Shah, G. Shin, S. M. Radha, and I. J. Yoon, "A Compact triple-band antenna with a broadside radiation characteristic for head-implantable wireless communications", *IEEE Antennas and Wireless Propagation Letters*, vol. 20, no. 6, pp. 958-962, 2021.

[17] W. Cui, Z. Li, C. Fan, M. Wang, H. Zheng, and E. Li, "Design of circularly polarized implantable antenna for wireless intracranial pressure monitoring system", *International Journal of RF and Microwave Aided-Computer Engineering*, vol. 32, no. 4, pp. 1-12, 2022.

[18] Z. Yudi, L. Changrong, L. Xueguan, Z. Ke, and Y. Xinmi, "A Wideband circularly polarized implantable antenna for 915 Mhz ISM-band biotelemetry devices", *IEEE Antennas and Wireless Propagation Letters*, vol. 17, no. 8, pp. 1473-77, 2018.

[19] L. J. Xu, Z. J. Chu, L. Zhu, J. P. Xu, and Z. Duan, "Design and analysis of dual-band implantable antennas based on effective relative permittivity calculation", *IEEE Transaction on Antennas and Propagation*, vol. 69, no. 5, pp. 2463-2472, 2021.

[20] Y. Feng, Y. Li, and L. Li, "Design and system verification of reconfigurable matching circuits for implantable antennas in tissues with broad permittivity range", *IEEE Transaction on Antennas and Propagation*, vol. 68. no. 6, pp. 4955-60, 2020.

[21] M. Palandoken, "Compact bioimplantable MICS and ISM band antenna design for wireless biotelemetry applications", *Radioengineering*, vol. 26, no. 4, pp. 917-23, 2017.

[22] K. Yeap, C. Voon, T. Hiraguri, and H. Nisar, "A Compact dual-band implantable antenna for medical telemetry", *Microwave and Optical Technology Letters*, vol. 61, no. 9, pp. 2105-09, 2019.

[23] A. E. Mohamed, M. S. Sharawi, and A. Muqaibel, "Implanted dual-band circular antenna for antenna for biomedical applications", *Microwave and Optical Technology Letters*, vol. 60, pp. 1125-32, 2019.

[24] D. Nguyen and C. Seo, "An Ultra-Miniaturized Antenna Using Loading Circuit Method for Medical Implant Applications", *IEEE Access*, vol. 9, pp. 111890-111898, 2021.

[25] F. Yang, L. Zhaonan, Q. Lin, S. Wanting, and L. Gaosheng, "A compact and miniaturized implantable antenna for ISM band in wireless cardiac pacemaker system", *Nature Scientific Reports*, vol. 12, no. 238, 2022.

Received 20 March 2022

Ömer Faruk Çelik was born in Antalya, Turkey, in 1993. He received the BS and MS degrees from Karadeniz Technical University at Electrical and Electronics Engineering in 2017 and Akdeniz University in Electrical and Electronics Engineering in 2021, respectively. He has been continuing PhD at Karadeniz Technical University in Electrical and Electronics Engineering since 2021. He has been a Research Assistant in department of Electronics and Communication Engineering, Karadeniz Technical University, Trabzon Turkey since 2021. His research interests include implantable antennas, frequency reconfigurable antennas, and antennas for cognitive radio communication.

Sıddık Cumhur Başaran was born in Bayburt, Turkey, in 1975. He received the BS, MS, and PhD degrees from the Kocaeli University, all in electronics and communication engineering, in 1996, 2000, and 2008, respectively. During 2011 to 2012, he was a visiting scholar at the Ohio State University, Electroscience Laboratory. He has been an Associate Professor in the Department of Electrical-Electronics Engineering, Akdeniz University, Antalya, Turkey since 2017. His research interests include fix and reconfigurable microstrip antenna, planar antennas for implantable applications, design of biotelemetry device and biomedical wireless communication.